1-1-2022

Impacts of atmospheric stilling and climate warming on cyanobacterial blooms: An individual-based modelling approach

Mohammad Hassan Ranjbar

David P. Hamilton

Amir Etemad-Shahidi
Edith Cowan University, a.etemadshahidi@ecu.edu.au

Fernanda Helfer

Impacts of atmospheric stilling and climate warming on cyanobacterial blooms: An individual-based modelling approach

Mohammad Hassan Ranjbar [a], David P. Hamilton [b,*], Amir Etemad-Shahidi [a,c], Fernanda Helfer [a]

[a] *School of Engineering and Built Environment, Griffith University, QLD 4222, Australia*
[b] *Australian Rivers Institute, Griffith University, QLD 4111, Australia*
[c] *School of Engineering, Edith Cowan University, WA 6027, Australia*

ABSTRACT

Harmful algal blooms of the freshwater cyanobacteria genus *Microcystis* are a global problem and are expected to intensify with climate change. In studies of climate change impacts on *Microcystis* blooms, atmospheric stilling has not been considered. Stilling is expected to occur in some regions of the world with climate warming, and it will affect lake stratification regimes. We tested if stilling could affect water column *Microcystis* distributions using a novel individual-based model (IBM). Using the IBM coupled to a three-dimensional hydrodynamic model, we assessed responses of colonial *Microcystis* biomass to wind speed decrease and air temperature increase projected under a future climate. The IBM altered *Microcystis* colony size using relationships with turbulence from the literature, and included light, temperature, and nutrient effects on *Microcystis* growth using input data from a shallow urban lake. The model results show that dynamic variations in colony size are critical for accurate prediction of cyanobacterial bloom development and decay. Colony size (mean and variability) increased more than six-fold for a 20% decrease in wind speed compared with a 2 °C increase in air temperature. Our results suggest that atmospheric stilling needs to be included in projections of changes in the frequency, distribution and magnitude of blooms of buoyant, colony-forming cyanobacteria under climate change.

1. Introduction

Surface water temperature of many lakes and reservoirs around the world are increasing as a result of climate change (O'Reilly et al., 2015). Increases in temperature affect many biogeochemical processes and produce compositional shifts in fish species (Sharma et al., 2007), changes in lake primary productivity (O'Reilly et al., 2003) and alterations to zooplankton grazing rates (Williamson et al., 2010). Increases in temperature can also promote cyanobacteria blooms (Paerl and Huisman, 2008), and may lead to increases in the production of cyanobacterial toxins (Wood et al., 2015). Increases in temperature affect cyanobacteria bloom frequency and magnitude in multiple ways (Jöhnk et al., 2008; Paerl and Huisman, 2008). Cyanobacteria generally have optimal growth rates and proliferate rapidly at elevated temperature (Thomas and Litchman, 2016). Warming of lake surface water increases stratification strength and duration (Kirillin, 2010; Butcher et al., 2015), reducing water column turbulence (Hozumi et al., 2020). As buoyant cyanobacteria disentrain with reduced turbulence, they accumulate at the water surface and form blooms (Humphries and Imberger, 1982).

Microcystis aeruginosa – the most prevalent toxin-producing, bloom-forming cyanobacterium – is frequently associated with seasonally or intermittently thermally stratified freshwater bodies (Robarts and Zohary, 1984; Brookes and Ganf, 2001).

Atmospheric stilling (the decrease in near-surface wind speed) amplifies density stratification in lakes as it reduces the momentum and mechanical energy fluxes across the lake-air interface and, in turn, the degree of vertical mixing (Woolway et al., 2017; Woolway and Merchant, 2019). Increased density stratification impacts cyanobacteria in several ways. For instance, reduced levels of turbulent mixing may no longer suppress vertical migration of colonies (Visser et al., 2016). Turbulence also affects cyanobacteria colony size (O'Brien et al., 2004; Regel et al., 2004). Laboratory and field observations have shown high levels of aggregation of *M. aeruginosa* cells and colonies exposed to low levels of turbulence (Regel et al., 2004; Qin et al., 2018) while high rates of turbulent mixing reduce colony size of *M. aeruginosa* through disaggregation (O'Brien et al., 2004; Li et al., 2018).

The cyanobacterium *Microcystis* can form colonies of different shapes and sizes (Li et al., 2018; Xiao et al., 2018). Colonial morphology of

---

* Corresponding author.
E-mail address: david.p.hamilton@griffith.edu.au (D.P. Hamilton).

Microcystis is a key physiological trait (Duan et al., 2018) that enables increases in the rate of vertical migration and formation of larger blooms during calm periods (Xiao et al., 2018). However, the formation of colonies reduces the maximum cell growth rate compared with solitary cells (Xiao et al., 2018). Extracellular polymeric substances (EPS) produced by *Microcystis* enhance colony formation (Yang et al., 2008), allowing cells to stick together and form larger colonies (Xiao et al., 2017, 2019). Various abiotic and biotic factors affect EPS and, in turn, colony formation. For example, flagellate grazing can increase the production of EPS by *M. aeruginosa*, leading to the formation of larger colonies that are less susceptible to grazing (Burns, 1968; Yang et al., 2008). In addition, *Microcystis* exposed to heavy metals increases the secretion of EPS to precipitate the metal ions, causing colony formation (Xiao et al., 2018). Increases in colony size affect *Microcystis* through protection against predators, as large colonies are not easily ingested by zooplankton. Colony size also has a major effect on the vertical migration velocity because, according to Stokes' law, and at low Reynolds' numbers, the velocity varies with the colony diameter squared (Reynolds, 1997). Aggregated (large) colonies therefore have greater buoyancy, allowing higher rates of migration to the surface than smaller colonies (Qin et al., 2018). Colony morphology also affects vertical velocity, with different 'morphospecies' characterised by a variety of shapes and sizes (Li et al., 2016, 2018), allowing them to float or sink more slowly than spherical colonies (Reynolds, 1997).

A number of modelling studies have attempted to simulate the vertical distribution of *Microcystis* colonies, most using a specific colony size (Wallace et al., 2000; Aparicio Medrano et al., 2013; Yao et al., 2017) whilst acknowledging that colony size has a significant effect on the vertical distributions. Colony size varies dynamically in space and time, depending upon external forcings (Lin et al., 2015). For example, Ibelings et al. (1991) measured *Microcystis* colony size distribution near the surface and at 8 m depth in Lake Vinkeveen, the Netherlands. They reported that the proportion of the largest size classes increased near the surface, whereas the smallest size classes dominated at 8 m. Large buoyant colonies resulting from aggregation are the most important for *Microcystis* surface scum formation (Robarts and Zohary, 1984; Wu et al., 2020), and the time required for scums to form is influenced by the size of large colonies in the water column as they constitute the majority of the biomass in scums (Hozumi et al., 2020). Colony accumulation near the water surface can increase growth rates because of favourable environmental conditions at the surface (e.g., light availability), extending the duration of persistence of surface scums (Hozumi et al., 2020).

Light affects the vertical distribution of *Microcystis* colonies through accumulation of starches that act as ballast (Wu and Kong, 2009). Ibelings et al. (1991) reported that the density of *Microcystis* colonies usually increases during the day, resulting in sinking, and decreases at night, resulting in floatation. This behaviour, however, is largely influenced by the colony size, as demonstrated by Wu and Kong (2009). By examining the vertical distribution of *M. aeruginosa* colonies of different sizes, these authors reported that large colonies (>120 μm) remained at the surface regardless of wind and light conditions, while small colonies (<36 μm) were distributed uniformly in the water column under strong winds and migrated to greater depths (to avoid high light intensities) under gentle winds. Colonies between 36 and 120 μm remained in the surface layer on calm days, irrespective of the levels of solar radiation. Measurements of *Microcystis* colony size distribution in Lake Erie (USA-Canada) showed that colonies were typically >50 μm and buoyant (Vanderploeg et al., 2001; Rowe et al., 2016). Qin et al. (2018) reported that the floating velocity of colonies with diameter from 100 to 425 μm was about 1500 times greater than that of colonies with diameter <20 μm. It has been hypothesised that large colonies remain buoyant because of low light availability in the colony interior, preventing the accumulation of carbohydrate ballast (Qin et al., 2018), but gas bubbles growing on or within the mucilage of colonies may also explain buoyancy in surface blooms (Aparicio Medrano et al., 2016).

For prediction of cyanobacteria blooms, previous studies have highlighted the importance of incorporating (1) vertical mixing and factors impacting site-specific turbulence levels, such as wind and surface cooling/heating (Wynne et al., 2013; Hozumi et al., 2020), (2) variability in the colony size distribution as a function of aggregation and disaggregation of colonies (O'Brien et al., 2004; Wu and Kong, 2009; Aparicio Medrano et al., 2013; Hozumi et al., 2020; Wu et al., 2020), and (3) variations in growth rate (Hozumi et al., 2020). Tradiional (e.g., population-level) models, are unable to collectively consider these processes as populations are lumped into state variables that are assumed to have uniform features. Individual-based models (IBMs) are able to incorporate these key processes and capture the heterogeneity of populations, and thus, better predict the dynamics of *Microcystis* blooms (Ranjbar et al., 2021).

In this study, we developed an IBM that incorporated the key processes controlling the development, persistence and disappearance of *Microcystis* blooms. This model was coupled with a three-dimensional hydrodynamic model to capture the horizontal and vertical distributions of *Microcystis*. For the first time, we show how colony size changes dynamically and continuously in response to environmental conditions such as the turbulent mixing intensity and temperature. Capturing these processes enables us to quantify the potential impacts of atmospheric stilling and warming air temperature on *Microcystis* blooms. We hypothesized that *Microcystis* bloom formation would be enhanced by the combination of increased growth rate at higher temperatures, and increased colony aggregation because of reduced levels of turbulence under a warmer and calmer future climate.

2. Methods

2.1. Study site

The model was applied to Forest Lake ($-27.622°$ S, $152.965°$ E) in Southeast Queensland, Australia. The lake is an urban setting and was constructed in early 1993. Forest Lake has an area of about 10 ha, and a maximum depth of around 4 m (Fig. 1). The lake acts as both a sedimentation basin for stormwater runoff and a recreational water body. It has four inflows entering from the northwest and south, and it drains through three bell-mouth spillways located in the northeast of the lake (Fig. 1). The lake receives stormwater runoff from its upstream urban catchment of 280 ha. To manage the water level in the lake during heavy runoff, the spillways release excess water only after the lake reaches its maximum capacity.

2.2. Modelling system

A three-dimensional (3D) hydrodynamic model and an IBM were used to simulate the hydrodynamics of the lake and incorporate the *Microcystis* population (Fig. S1). The hydrodynamic model was run under atmospheric and discharge forcings and the IBM was then forced by the outputs of the hydrodynamic model. The IBM consisted of three sub-models that included rate of colony size change, growth in relation to light, nutrients, and temperature, and buoyancy for size-dependant vertical movement (Fig. S1).

2.2.1. Hydrodynamic (lake) model
The MIKE 3 Flow Model FM 3D model used in this study is based on a numerical solution of the 3D incompressible Reynolds Averaged Navier–Stokes equations, subject to the assumptions of Boussinesq and hydrostatic pressure. The spatial discretisation is performed using a cell-centred finite volume method. The horizontal eddy viscosity is estimated using the Smagorinsky formulation and the vertical eddy viscosity with the k-epsilon formulation. The model includes meteorological forcings to simulate the major heat fluxes including latent heat flux (evaporation), sensible heat (convection), short wave radiation, and long wave radiation (DHI, 2021). The model has been widely used in
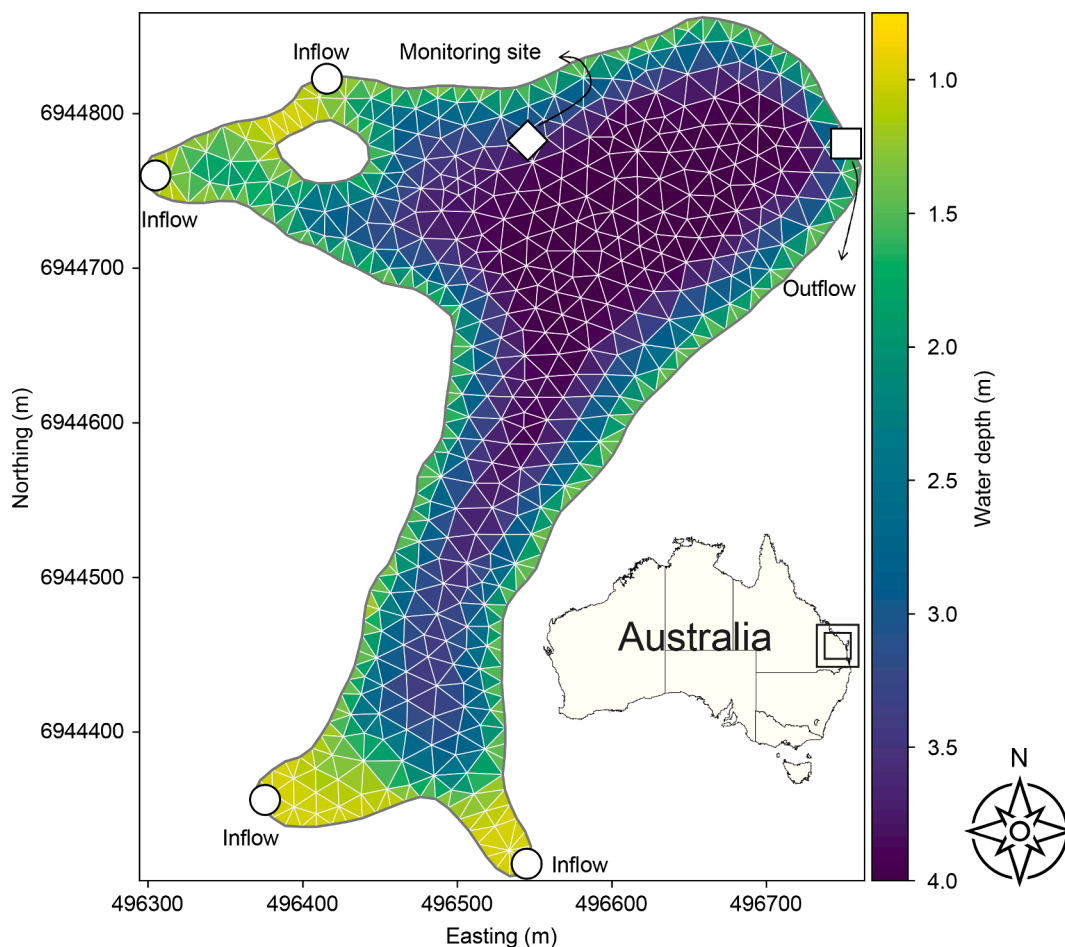
Fig. 1. Bathymetry of Forest Lake and mesh distribution for model set-up. The circles, squares, and rhombi indicate the locations of inflows, outflow, and monitoring site, respectively. The coordinate system refers to UTM-56 J zone. Inset: location of Forest Lake in Queensland, Australia.

hydrodynamic modelling (e.g., Sokolova et al., 2013; Wood et al., 2020; Zhang et al., 2020) and previous studies have demonstrated its ability to simulate accurately the hydrodynamic and thermal structure of inland water bodies (Sokolova et al., 2013; Zhang et al., 2020).

The model takes fixed data for lake bathymetry and uses meteorological variables, inflow discharge and temperature, and outflow discharge to simulate lake hydrodynamics. Bathymetry data were collected from Brisbane City Council (BCC). The meteorological data required to run the model consist of air temperature, wind speed and direction, short and long wave radiation, precipitation, evaporation, and relative humidity. All data other than short and long wave radiation were obtained from the Bureau of Meteorology Archerfield Airport station (27.57° S, 153.01° N) approximately 7 km northeast of the study area. These data were measured every 10 min. Hourly short and long wave radiation data were obtained from the ERA5 reanalysis product available at a spatial resolution of 0.25°. Chowdhury et al. (2012) measured rainfall-runoff in the Forest Lake catchment. A measured runoff volume of 42% of the rainfall volume in the catchment was adopted in our study. The inflow temperature was estimated based on the air temperature (Zhang et al., 2020).

The computational domain for the model was composed of an unstructured triangular grid with 920 elements and 561 nodes (Fig. 1). The horizontal resolution of the triangular grids was approximately 20 m. The 3D domain comprised a combined sigma/z-level vertical distribution with 20 layers to provide a vertical resolution of 0.2 m.

In this study, the light extinction coefficient (K_d) was estimated as (Huisman et al., 2004):

$$K_d = K_{bg} + c \times K_i \tag{1}$$

where K_{bg} is background turbidity, c is the cell concentration of *Microcystis* colonies, and K_i is a *Microcystis*-specific light extinction coefficient. Following Huisman et al. (2004), K_{bg} and K_i were set to 0.6 m^{-1} and 3.4×10^{-12} m^2 cell^{-1}, respectively.

Phycocyanin fluorescence was measured at 15 min intervals near the centre of Forest Lake (Fig. 1) with a YSI 6131 blue-green algae sensor (Yellow Springs Instruments, Yellow Springs, Ohio, USA). Water samples for phytoplankton cell counts were collected in the lake on 8 sample days. Correlations between biovolume and cell counts for cyanobacteria species developed by Rousso et al. (2022) were used to determine cyanobacteria biovolume. The biovolume data showed that *Microcystis* spp., mostly *Microcystis aeruginosa*, were dominant before and after the bloom that occurred during our study. For example, *Microcystis* spp. accounted for 85% of the total cyanobacteria biovolume on the 28 February 2020. We established a relationship between phycocyanin fluorescence and biovolume (from cell counts) (Fig. S2). This relationship was used to convert phycocyanin fluorescence to an equivalent cell count (Fig. 4a). The cell counts were used to determine the light extinction coefficient based on Eq. (1).

2.2.2. Individual-based model (IBM)

An IBM was developed in the MIKE ABM Lab environment (DHI, 2021) to simulate the growth, aggregation, disaggregation, vertical migration velocity, and three-dimensional advection of *Microcystis* colonies. The model conserves cyanobacteria mass. The aggregation of colonies leads to a decrease in biomass of small colonies while disaggregation increases the biomass of small colonies. In the IBM, the growth model parameters included the maximum daily growth rate of the colonies at 20 °C (μ_{max}) as a function of colony surface area (s in μm^2) to volume (v in μm^3) (Reynolds, 1989):

$$\mu_{max} = 1.142\left(sv^{-1}\right)^{0.325} \tag{2}$$

The net daily growth rate (μ_{net}) was governed by the following equation:

$$\mu_{net} = \mu_{max}f(T)f(I)\min[f(N),f(P)] - Rv^{(T-20)} \tag{3}$$

where $f(T)$, $f(I)$, $f(N)$, and $f(P)$ are functions applied to regulate growth dependence on temperature, light, nitrogen, and phosphorus concentrations, respectively, T is water temperature, R is a term that represents the combined effect of respiration and mortality at 20 °C, and v is a constant governing the respiration response to water temperature. In line with Robson and Hamilton (2003), R and v were set to 0.1 and 1.1 d^{-1}, respectively. The temperature response function was applied to the growth rate as a multiplicative factor and is an Arrhenius function which allows inhibition above an optimal temperature (Robson and Hamilton, 2003). In this modelling study, "Liebig's law of the minimum" was considered for limitation by N or P at any time, using a Michaelis–Menten function for each nutrient:

$$f(P) = P/(K_P + P) \tag{4}$$

$$f(N) = N/(K_N + N) \tag{5}$$

where K_P and K_N are the half-saturation constants for P and N limitation, respectively. K_P and K_N were set to 0.003 mg P L^{-1} and 0.025 mg N L^{-1}, respectively (Guven and Howard, 2006). P (the concentration of phosphate) and N (the sum of ammonium and nitrate concentrations) were determined from field data measured by BCC in Forest Lake.

To consider light limitation, first, the surface irradiance (I_0) at different times was calculated from shortwave radiation. After correcting for surface albedo (8%), 43% of shortwave radiation was assumed to be photosynthetically active (Pinker and Laszlo, 1992). The irradiance (I_z) that a colony was exposed to at depth z was then estimated by Lambert-Beer's law of exponential light extinction:

$$I_z = I_0 e^{-K_d z} \tag{6}$$

Finally, the limitation term for light was described by a Michaelis–Menten equation:

$$f(I) = I_z/(K_I + I_z) \tag{7}$$

where K_I is the half-saturation constant for light limitation that was set to 25 µmol m^{-2} s^{-1} in line with Guven and Howard (2006). In the IBM, any control of biomass by grazers was ignored as the colonial form of *M. aeruginosa* results in limited grazing (Böing et al., 1998).

Based on the net daily growth rate, the doubling time (D_{time}), and colony size changes resulting from growth ($D_{G,t}$) at the current time step (t), were calculated as:

$$D_{time} = \frac{\ln(2)}{\mu_{net}} \tag{8}$$

$$D_{G,t} = D_{t-1} \times 2^{\frac{\Delta t}{D_{time}}} \tag{9}$$

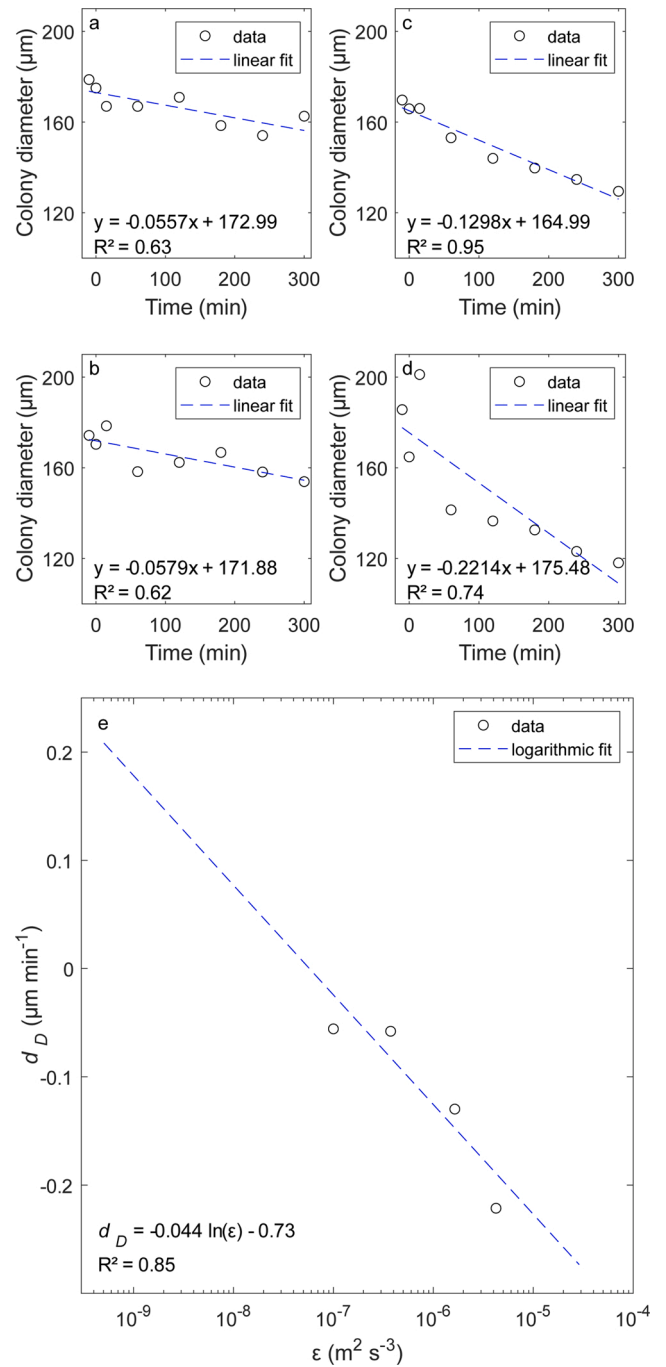where D_{t-1} is the colony size at the previous time step ($t-1$) and Δt is the time interval.

Fig. 2. (a–d) *M. aeruginosa* colony diameter versus time for four different ranges of turbulent dissipation (ε of 5×10^{-9} to 9×10^{-5} m^2 s^{-3}) (for details see O'Brien et al., 2004); (e) rate of change in colony diameter of *Microcystis* versus mid-point of the range of $\log_{10}(\varepsilon)$. The equations for best-fit lines and the R-squared values are shown in panels.

To determine the response of colony size change to turbulent mixing, the experimental results of O'Brien et al. (2004) were used. They conducted six experiments where *M. aeruginosa* samples were exposed to a range of turbulent dissipation values (ε), with colony diameter measured over time (Fig. 2a–d). A linear fit was applied to describe each observation, and the slope of the fit of colony diameter with time was taken as the rate of change of colony size (d_D) for each experiment (Fig. 2a–d). Two of the experiments from O'Brien et al. (2004) which had no clear trend in d_D were not included.

To develop a function for the rate of change of colony size with

turbulent dissipation, the rates of colony size change were plotted against turbulent dissipation (Fig. 2e). A logarithmic trendline was fitted to the data points, and its equation was used as the rate of diameter change (d_D) in the IBM:

$$d_D = -0.044\ln(\varepsilon) - 0.73 \tag{10}$$

According to Eq. (10), turbulent dissipation $> 5.76 \times 10^{-8}$ m^2 s^{-3} results in colony disaggregation and below this level leads to colony aggregation.

As seen in Fig. 2e, there were no data for low values of the turbulent dissipation, ε. Therefore, to understand the impact of the potential errors derived from extrapolating the aggregation rate, a sensitivity analysis of the aggregation rate in the IBM was performed. The effect of selecting different aggregation rates was small, and the general pattern of the modelled cell concentration remained similar. After calculating (d_D), the colony diameter was updated as:

$$D_t = D_{G,t} + (d_D \times \ \Delta t) \tag{11}$$

where D_t is the colony diameter at the end of each time step.

After simulating colony growth and aggregation or disaggregation, the vertical migration velocity of a colony (w_s) was estimated in the IBM based on Stokes' Law:

$$w_s = \frac{gD^2(\rho_w - \rho_{col})}{18\varphi\mu} \tag{12}$$

where g is the acceleration of gravity, ρ_w is the density of water, ρ_{col} is the density of a colony, φ is the shape coefficient and μ is the dynamic viscosity of water. Reynolds et al. (1987) uses a shape coefficient of 1 for *M. aeruginosa* < 240 μm diameter. Therefore, φ was set to 1 in the IBM as the modelled colonies were < 240 μm. In addition, colonies were assumed to be buoyant, in line with Rowe et al. (2016). Reynolds et al. (1987) also showed that the density of *M. aeruginosa* < 240 μm is between 985 and 1005 kg m^{-3}. We fixed the density difference between the water and colonies at 10 kg m^{-3} as our focus was on the effect of changes in the colony size and growth rate of *Microcystis*. The colonies were advected by the flow field and dispersed by turbulence. The flow field and turbulent diffusivity were obtained from the lake model (Fig. S1). The transport of each colony depends on the interaction between its vertical migration velocity, advection, and dispersion as discussed by Ranjbar et al. (2021).

To compare the model results with measured *Microcystis* cell concentrations, the diameter of a colony, which is influenced by growth, aggregation, and disaggregation, was used to estimate the number of cells within the colony. Since *Microcystis* colonies have a fractal structure (Li et al., 2018), the following equation was used to determine the number of the constituent cells (i) of a colony with a diameter of D:

$$i = \left(\frac{De}{D_0}\right)^{D_f} \tag{13}$$

where e is the porosity coefficient, D_0 is the diameter of a *Microcystis* cell (5 μm), and D_f is the fractal dimension (set to 2.5; Nakamura et al., 1993). As the porosity of colonies increases with an increase in the colony diameter (Nakamura et al., 1993), the porosity coefficient was varied linearly from 1 for single cells to 0.2 for the largest *Microcystis aeruginosa* colonies (Aparicio Medrano et al., 2013; Xiao et al., 2018).

One of the main limitations of IBMs is their complexity and high computational demand in modelling large systems where there are a large number of species (Ranjbar et al., 2021). For example, in Forest Lake, cell counts of *Microcystis* exceeded 3.7×10^5 cells mL^{-1} (Fig. 4a), and it is not feasible to simulate each individual. To overcome this limitation, super individual-based modelling was used, in which a number of individuals are lumped into a single representative individual (Scheffer et al., 1995; Hellweger and Bucci, 2009; Hellweger et al., 2016).

2.2.3. Model evaluation

The performance of the hydrodynamic model was assessed using observed water temperature and current speed data. BCC provided measured water temperature at depths of 1 and 3 m taken at 15 min intervals with a YSI 6560 temperature sensor. Current speed data was measured with a Vector Acoustic Doppler Velocimeter (ADV; Nortek, Norway). The ADV sampled velocity at 64 Hz and operated in burst mode, collecting 4096 samples per burst (every 30 min). The performance of the IBM was also evaluated against *Microcystis* cell concentrations calculated from phycocyanin fluorescence measurements at depth of 1 m. The cell count data are discussed earlier in Section 2.2.1.

2.3. Atmospheric stilling and climate warming scenarios

Previous studies showed that long-term wind speed trends over Australia have been -0.009 (McVicar et al., 2008) and -0.010 m s^{-1} yr^{-1} (Donohue et al., 2010). These trends would equate to a 20% decrease in wind speed by 2100. We chose a decrease of wind speed of up to 20% of the measured wind speed in January and February 2020, the period when the model was applied to Forest Lake.

The Queensland Department of Environment and Science provides dynamically downscaled high-resolution (~10 km spatial resolution) climate projections from the fifth phase of the Coupled Model Intercomparison Project (CMIP5) multi-model database (Syktus et al., 2020). Projections are based on both moderate- and high-emissions scenarios, i.e., Representative Concentration Pathways 4.5 and 8.5 (RCP4.5 and RCP8.5, respectively). These downscaled projections show that the average rise in air temperature by 2100 in Southeast Queensland would be between 1 and 5 °C. The projections were used as a basis to select a range of plausible temperature increases, up to $+5$ °C of the measured air temperature in January and February 2020.

3. Results

3.1. Model calibration

The hydrodynamic model was calibrated and validated against measured water temperature at depths of 1 and 3 m. Following Sokolova et al. (2013), the settings for the minimum and maximum vertical eddy viscosity were adjusted to accurately reproduce the temperature gradient at the observed depths. The minimum and maximum vertical eddy viscosities were set to 1.0×10^{-7} and 1.0×10^{-5} m^2 s^{-1}, respectively. The convective heat transfer coefficient between the water and the atmosphere was set to 0.007 to accurately reproduce lake water surface temperature. Two statistical measures were used to assess model performance: correlation coefficient (R) and root mean square error (RMSE). As seen in Fig. 3, simulated water temperatures agreed well with measurements during the calibration (29 Dec 2019–18 Jan 2020) and validation period (18 Jan–5 Feb 2020).

The hydrodynamic model was also calibrated using measured current speed data. The wind drag coefficient that affects the surface water stress was tuned in the hydrodynamic model to obtain agreement with measured data. In the lake model, the drag coefficient depends on the wind speed as follows:

$$c_d = \begin{cases} c_a & w_{10} < w_a \\ c_a + \dfrac{c_b - c_a}{w_b - w_a}(w - w_a) & w_a \le w_{10} \le w_b \\ c_b & w_{10} > w_b \end{cases} \tag{14}$$

where c_d is the drag coefficient and w is wind speed. c_a, c_b, w_a, and w_b are empirical factors that were set to 0.0004, 0.0025, 7 m s^{-1}, and 25 m s^{-1}, respectively. Simulated time series of the current speed were compared with those of the measured data using values of R and RMSE as model performance indicators (Table 1).

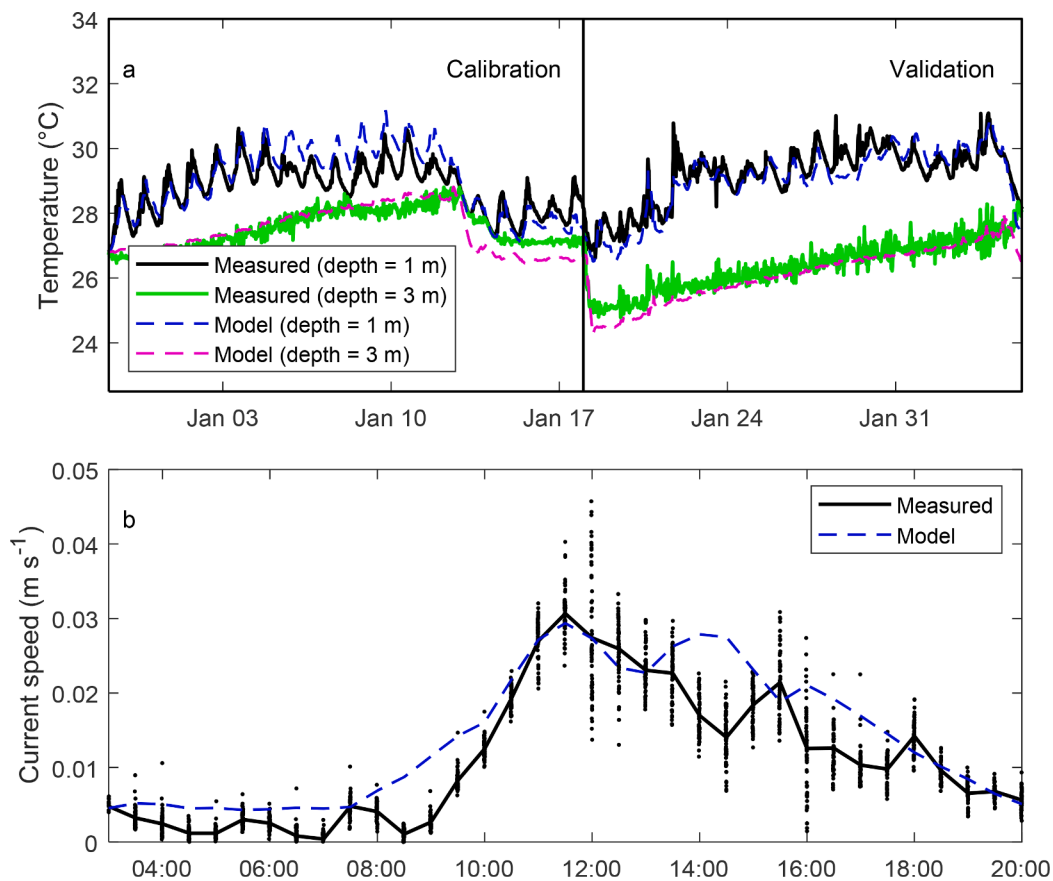Fig. 4a shows the variations in *Microcystis* cell concentration

Fig. 3. Comparison between measured (continuous line) and modelled (dashed line) water temperature from 29 December 2019 through 5 February 2020 (a) and current speed (24-h clock) on 22 June 2020 (b). The dots and lines in the bottom plot represent actual and 1-min average data, respectively.

Table 1

Lake model performance (correlation coefficient, R, and root mean square error, RMSE) for water temperature at different depths during the calibration period (29 December 2019–18 January 2020) and validation period (18 January 2020–5 February 2020), and for current speed during the calibration period (22 June 2020).

Variable	R	RMSE
Temperature at 1 m (calibration)	0.90	0.54 °C
Temperature at 3 m (calibration)	0.85	0.37 °C
Temperature at 1 m (validation)	0.91	0.45 °C
Temperature at 3 m (validation)	0.93	0.40 °C
Current speed	0.91	0.005 m s^{-1}

calculated from phycocyanin fluorescence measurements between 27 Jan 2020 and 6 Feb 2020. During this period, *Microcystis* concentrations exceeded 3.7×10^5 cells mL^{-1} and then decreased to around 7×10^4 cells mL^{-1}. Fig. 4a also compares the calculated and modelled *Microcystis* cell concentration. A RMSE of 0.7×10^5 cells mL^{-1} and correlation coefficient of 0.66 were noted between the model results and observations. To understand the effects of water column stability on the bloom formation and collapse, a time series of Schmidt stability (Idso, 1973) was generated based on the modelled water column profile of temperature. Schmidt stability denotes the energy required to fully mix the water column. The R package "rLakeAnalyzer" was used for the calculation of Schmidt stability (S_t; Winslow et al., 2019). As seen in Fig. 4b, the bloom developed during a period of high water-column stability and collapsed when water column stability decreased rapidly. Fig. 4c shows the average number of cells per colony in the top 1 m layer of Forest Lake. As a result of the formation of large colonial aggregates, there was an increase in the size of colonies near the water surface during the period of

high water-column stability, while the colony size decreased at low water-column stability (Fig. 4c). As a result of the high water-column stability and the ensuing colony aggregation, more colonies accumulated near the water surface (Fig. 4d) where elevated water temperature and high photosynthetically active radiation (PAR) promoted increased rates of growth (Fig. 4e, f). From these results it was concluded that a combination of high S_t, high PAR, and near-optimal temperature for the growth of *Microcystis* supported the bloom formation. On the other hand, during mixing events ($S_t < 5$), colonies were redistributed in the water column (Fig. 4d) and encountered cooler temperatures and low PAR (Fig. 4e, f). Note that growth of *Microcystis* was affected by temperature, light, and nutrient limitation, although K_P varied only between 0.7 and 0.76, and K_N varied between 0.73 and 0.75.

To demonstrate the importance of incorporating the colony size change in modelling the dynamics of colony-forming cyanobacteria, we ran scenarios in which colony size was assumed to be constant, and the average colony depths have been plotted in Fig. 5. Model results show that large colonies disentrained from the turbulent mixing and accumulated in near-surface waters while small colonies were entrained during the simulation period (Fig. 5). However, colonies whose size was changed dynamically experienced both entrainment and disentrainment in response to environmental conditions (e.g., turbulent dissipation and water temperature) (Fig. 5).

3.2. Atmospheric stilling and climate warming simulations

We modelled the response of *Microcystis* to variations in wind speed and air temperature. Fig. 6a shows that a decrease in wind speed produces larger colonies. The largest colonies were formed with the largest reduction (20%) in wind speed. The 20% reduction produced a 38% increase in the mean colony size and an increase of 37% in the colony
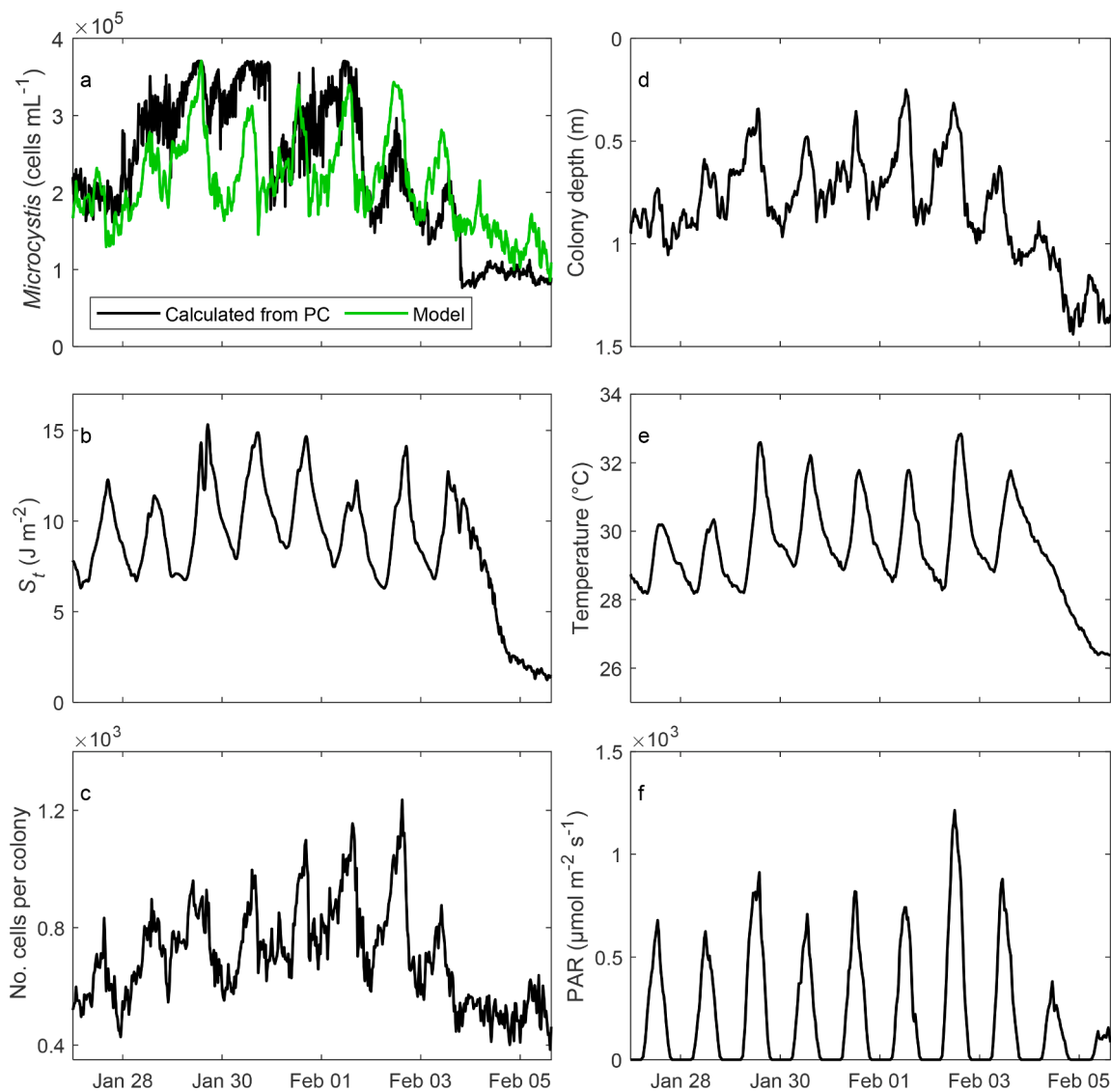
Fig. 4. Comparison between observed and modelled *Microcystis* cell concentration (a), Schmidt stability (b), number of cells per colony in the top 1 m layer of Forest Lake (c), average colony depth (d), water temperature (e), and PAR (f) in 2020. The solid lines (e and f) denote the average water temperature and PAR that colonies experienced in each time step. *Microcystis* cell concentration (a) was estimated based on phycocyanin fluorescence measurements, while Schmidt stability (b) was calculated based on the modelled water column profile of temperature. Number of cells per colony (c), colony depth (d), water temperature (e), and PAR (f) were extracted from outputs of the IBM.

size range (Fig. 6a). Note that growth of *Microcystis* was affected by temperature, light, and nutrient limitation, although K_P varied only between 0.7 and 0.76, and K_N varied between 0.73 and 0.75. A 20% decrease in the wind speed would lead to a 14% decrease in the mean colony depth (i.e., colonies closer to the water surface) (Fig. 6b), reinforcing conditions favourable for colony growth (i.e., higher temperature and PAR) (Fig. 6c, d). The wind speed reduction and reduced mixing resulted in larger colonies with greater vertical migration velocity, with colonies disentraining from turbulent mixing to accumulate at the water surface (Fig. 6b).

The scenarios of increase in air temperature have a smaller influence on the colony size and colony distribution, than the scenarios of reduced wind speed (Fig. 6a, b). With increase of temperature and longer duration of stratification, colonies accumulated more easily at the water surface in a future warmer climate. The largest colonies were formed under a 2 °C (=7.6%) increase in the air temperature. Increasing air temperature by 2 °C would cause the mean colony depth to decrease by 4% (Fig. 6b). Climate warming provided a favourable environment for the increased growth of *Microcystis* and accumulation near the water

surface (Fig. 6c, d). For instance, a temperature increase of 2 °C would increase the average water temperature that colonies experienced to 31 °C (Fig. 6c) while the average water temperature that colonies experienced in the baseline scenario (i.e., no changes in air temperature and wind speed measured in January and February 2020) was 29.3 °C. The optimal temperature for growth was considered to be 31.6 °C (Methods and Fig. S3). Under the assumption of no light and nutrient limitation, a *Microcystis* colony of 75 μm in diameter would have a net daily growth rate of 0.59 d^{-1} in response to a water temperature of 31 °C, while the net daily growth would be 0.56 d^{-1} in response to a water temperature of 29.3 °C. As observed in Fig. 6a, a 2 °C increase in the air temperature is predicted to increase the average colony size and the size range of colonies by ~5%.

4. Discussion

We developed a dynamic, mechanistic IBM of *Microcystis* focusing on colony size changes in response to environmental conditions. Vertical mixing, variations in colony size influenced by the aggregation and
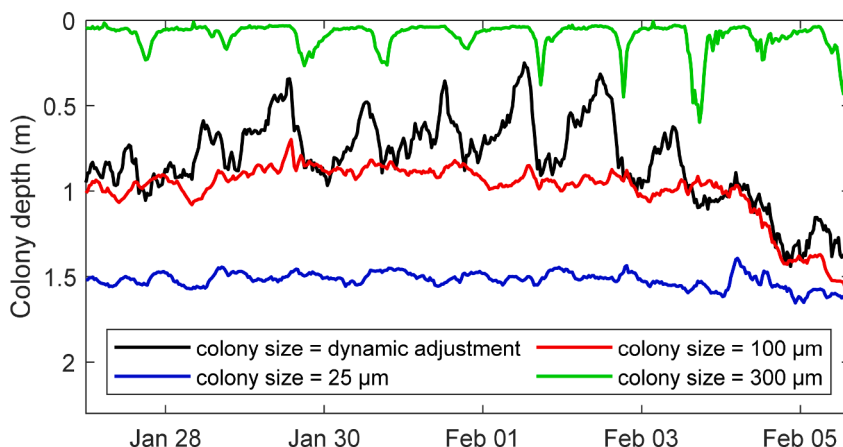
Fig. 5. Variations in modelled distribution of *Microcystis* colonies with different diameters in the water column in 2020. In three scenarios colony size was assumed to be constant, while in one scenario the colony size was changed dynamically in response to environmental conditions (e.g., turbulent dissipation and water temperature).
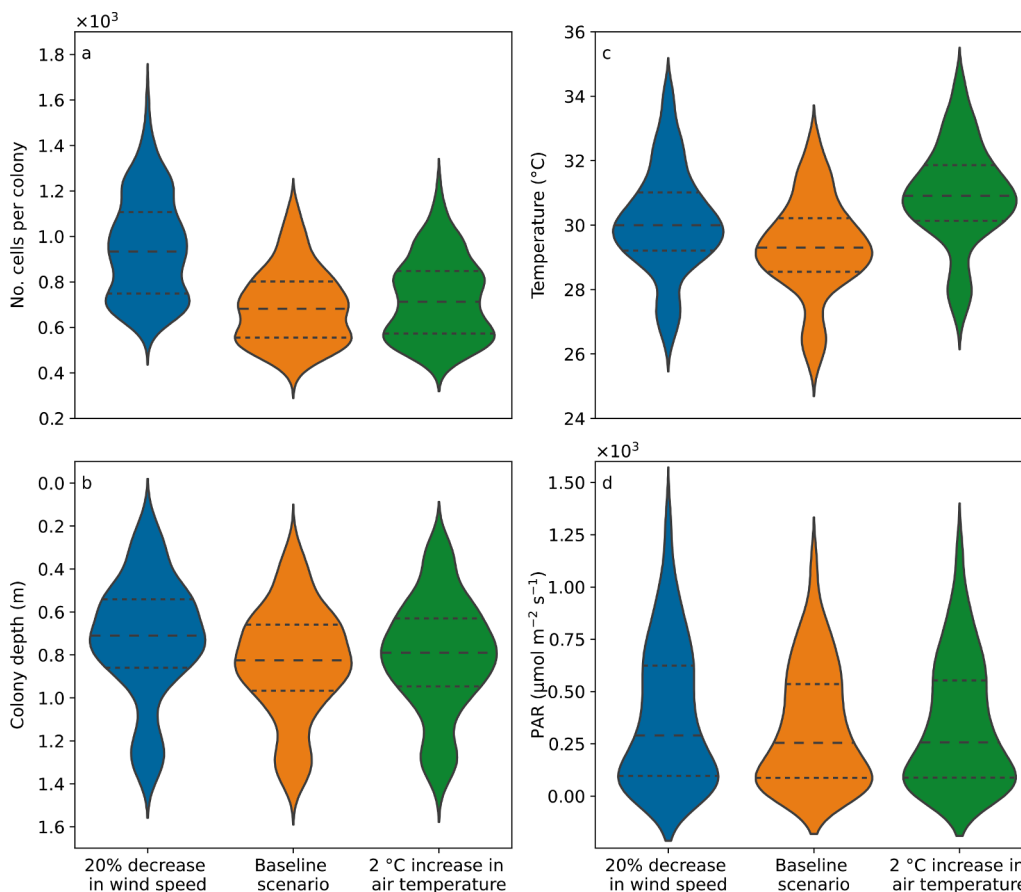

Fig. 6. Effects of the atmospheric stilling and climate warming on the modelled number of cells per colony (a), colony depth (b), water temperature (c), and PAR (d). The violin plots in (c) and (d) relate to what was experienced by the colonies during the simulation period.

disaggregation of colonies, and growth were incorporated into the IBM in line with the recommendations of previous studies (O'Brien et al., 2004; Wu and Kong, 2009; Aparicio Medrano et al., 2013; Wynne et al., 2013; Hozumi et al., 2020; Wu et al., 2020). Forced by currents, turbulent diffusivity, and water temperature from the lake model, the IBM simulated the development and distribution of *Microcystis* blooms. The results of the hydrodynamic model and the IBM (i.e., *Microcystis* cell concentration) were quantitatively compared with *in situ* high-frequency observations. The lake model reproduced accurately the

variation in measured water temperature and current speed, and the IBM captured the observed increase and decrease in *Microcystis* concentration in near-surface waters during diel stratification and during a mixing event, respectively. The agreement of IBM simulations with observed data provided confidence for use of the IBM to quantitatively examine the *Microcystis* bloom response to atmospheric stilling and warming.

Model results showed that during periods of low wind speed, colonies were exposed to low levels of turbulence. These colonies could

disentrain from the turbulence and accumulate near the water surface. As a result of low levels of turbulence, aggregation of colonies was predicted. In addition, lake model results showed that the low wind speeds in summer led to establishment of strong thermal gradients, creating a warm surface layer and a cooler bottom layer that reinforced conditions favourable for colony growth because large buoyant colonies remained in warm surface waters with high PAR. The average size of colonies continued to increase, with a decrease in maximum daily growth rates compared with the solitary (unicellular) *Microcystis*, according to the size-adjusted maximum daily growth rate (see Eq. (2)). Conversely, strong winds caused mixing events with high levels of turbulence that disaggregated colonies and reduced their buoyancy. Therefore, colonies were entrained in the turbulent mixing and became distributed through the water column. These smaller colonies were exposed to reduced water temperature and PAR levels compared with larger colonies in surface waters. Disaggregated (small) colonies and single cells grew quickly although they experienced lower temperature and PAR.

Rowe et al. (2016) and Wang et al. (2017) discuss how temporary stratification in shallow western Lake Erie and Lake Taihu, respectively, affects *Microcystis* vertical distributions. In line with these studies, our model results show that intermittent stratification plays an important role in bloom dynamics in our small, shallow polymictic lake. Previous IBM studies (Feng et al., 2018) discussed how wind-induced turbulence directly and indirectly affects *Microcystis* bloom dynamics. Direct effects relate to the entrainment of colonies and indirect effects are caused by entrained colonies that experience a different physical environment. However, turbulence has another effect that has not been incorporated in previous IBMs (or indeed any other system-scale models) of *Microcystis* blooms: turbulence-induced aggregation/disaggregation of colonies. These processes are critical for the formation and collapse of blooms as shown by Wu et al. (2020) in experimental work on the disproportionately large contribution of large colonies to surface scum formation by *Microcystis*.

Atmospheric stilling promotes the formation of large, buoyant colonies of *Microcystis* by enhancing colony aggregation and migration to the surface, to a greater extent that the simulated changes in air temperature. The abundance of large colonies may favour the development of persistent high-biomass blooms from large colonies with high buoyancy that disentrain from the turbulent mixing and accumulate in near-surface waters.

Most climate change projections for water quality focus on changes in temperature and indicate the critical importance of increased thermal stratification. Future projections based on temperature may have oversimplified other effects from climate change, however, and few models have considered wind speed, which is a sensitive driver of stratification. Similarly, we did not consider changes in rainfall with climate change. The effect of such a change would be altered hydrology as well as changes in nutrient loads and the proportions of different nutrient forms (Reichwaldt and Ghadouani, 2012; Hamilton et al., 2016). It is recommended that the focus of cyanobacteria predictions with climate change should extend beyond temperature and that climate-catchment-lake interactions as well as other variables (wind speed) be considered when assessing the impacts of climate change on bloom dynamics.

This study focused on *Microcystis aeruginosa* because *Microcystis* spp. dominate cyanobacteria blooms in freshwater ecosystems globally (78%) and *Microcystis aeruginosa* is the most commonly observed morphospecies (Xiao et al., 2020). While parameterisations may be specific to a particular morphospecies in this study, the same processes apply to other morphospecies and therefore the outcomes (associated with climate change) are likely to be similar, although there could be additional focus on succession of morphospecies under different turbulence regimes (Li et al., 2018).

The approach presented herein is a step forward to bridge the gap between current observational data and ecological models. Although observations show that *Microcystis* blooms are characterised by high levels of heterogeneity, population-level models still assume cyanobacteria populations are made up of identical individuals. We included the heterogeneity of colony size in our model, with colonies responding individually to environmental conditions (e.g., turbulent mixing). We also included formulations to describe growth responses to temperature, light, nutrients and colony size, which are important because of the trade-off between growth and buoyancy. Single cells and small colonies grow more quickly than large colonies. Building capability in IBMs requires development according to the prioritisation of the most important processes, as discussed in Ranjbar et al. (2021).

5. Conclusions

In this study, we coupled an IBM to the outputs of a 3D hydro-dynamic model to explicitly model colony size responses of cyanobacteria at full lake scale. The model developed for this purpose considers a high level of realism, including growth limitation due to nutrients, light and temperature. The modelling system reproduced the formation and collapse of a *Microcystis* bloom in a shallow subtropical lake. The inclusion of *Microcystis* colony aggregation/disaggregation processes, their growth and three-dimensional hydrodynamic processes in the model were important to capture bloom dynamics. The IBM developed in this study can be applied to model the dynamics of colony-forming cyanobacteria in other lakes, especially those with diurnal mixing or polymictic regimes (e.g., Lake Erie, USA-Canada, and Lake Taihu, China) that expose cells to changeable vertical gradients of turbulence. Our sensitivity analysis for air temperature and wind showed that atmospheric stilling has an important influence on cyanobacteria blooms. Trends in observed terrestrial near-surface wind speed show that atmospheric stilling is widespread worldwide. If this trend continues, especially in combination with rising temperatures and increasing loads of nutrients, there may be a substantial increase in the frequency and extent of cyanobacteria blooms globally, suggesting that water resource managers should consider the increased risk of cyanobacterial blooms under a warmer and calmer future climate.

Declaration of Competing Interest

The authors declare that they have no known competing financial interests or personal relationships that could have appeared to influence the work reported in this paper.

Data availability

Data will be made available on request.

Supplementary materials

Supplementary material associated with this article can be found, in the online version, at doi:10.1016/j.watres.2022.118814.

References

Aparicio-Medrano, E., Uittenbogaard, R.E., Dionisio-Pires, L.M., van de Wiel, B.J.H., Clercx, H.J.H., 2013. Coupling hydrodynamics and buoyancy regulation in *Microcystis aeruginosa* for its vertical distribution in lakes. Ecol. Model. 248, 41–56.

Aparicio Medrano, E., Uittenbogaard, R., van de Wiel, B., Pires, L.D., Clercx, H., 2016. An alternative explanation for cyanobacterial scum formation and persistence by oxygenic photosynthesis. Harmful Algae 60, 27–35.

Böing, W.J., Wagner, A., Voigt, H., Deppe, T., Benndorf, J., 1998. Phytoplankton responses to grazing by *Daphnia galeata* in the biomanipulated Bautzen reservoir. Hydrobiologia 389 (1), 101–114.

Brookes, J.D., Ganf, G.G., 2001. Variations in the buoyancy response of *Microcystis aeruginosa* to nitrogen, phosphorus and light. J. Plankton Res. 23 (12), 1399–1411.

Burns, C.W., 1968. The relationship between body size of filter-feeding Cladocera and the maximum size of particle ingested. Limnol. Oceanogr. 13 (4), 675–678.

Butcher, J.B., Nover, D., Johnson, T.E., Clark, C.M., 2015. Sensitivity of lake thermal and mixing dynamics to climate change. Climat. Change 129 (1), 295–305.

Chowdhury, R., Gardner, T., Gardiner, R., Hartcher, M., Aryal, S., Ashbolt, S., Petrone, K., Tonks, M., Ferguson, B., Maheepala, S., 2012. South East Queensland catchment modelling for stormwater harvesting research: instrumentation and hydrological model calibration and validation.

DHI, 2021. MIKE 3 Flow Model FM, Scientific Documentation. DHI Water & Environment.

Donohue, R.J., McVicar, T.R., Roderick, M.L., 2010. Assessing the ability of potential evaporation formulations to capture the dynamics in evaporative demand within a changing climate. J. Hydrol. (Amst) 386 (1), 186–197. -4.

Duan, Z., Tan, X., Parajuli, K., Upadhyay, S., Zhang, D., Shu, X., Liu, Q., 2018. Colony formation in two *Microcystis* morphotypes: effects of temperature and nutrient availability. Harmful Algae 72, 14–24.

Feng, T., Wang, C., Wang, P., Qian, J., Wang, X., 2018. How physiological and physical processes contribute to the phenology of cyanobacterial blooms in large shallow lakes: a new Euler-Lagrangian coupled model. Water Res. 140, 34–43.

Guven, B., Howard, A., 2006. Modelling the growth and movement of cyanobacteria in river systems. Sci. Total Environ. 368 (2), 898–908. -3.

Hamilton, D.P., Salmaso, N., Paerl, H.W., 2016. Mitigating harmful cyanobacterial blooms: strategies for control of nitrogen and phosphorus loads. Aquat. Ecol. 50 (3), 351–366.

Hellweger, F.L., Bucci, V., 2009. A bunch of tiny individuals Individual-based modeling for microbes. Ecol. Model. 220 (1), 8–22.

Hellweger, F.L., Clegg, R.J., Clark, J.R., Plugge, C.M., Kreft, J.U., 2016. Advancing microbial sciences by individual-based modelling. Nat. Rev. Microbiol. 14 (7), 461–471.

Hozumi, A., Ostrovsky, I., Sukenik, A., Gildor, H., 2020. Turbulence regulation of *Microcystis* surface scum formation and dispersion during a cyanobacteria bloom event. Inland Waters 10 (1), 51–70.

Huisman, J., Sharples, J., Stroom, J.M., Visser, P.M., Kardinaal, W.E.A., Verspagen, J.M., Sommeijer, B., 2004. Changes in turbulent mixing shift competition for light between phytoplankton species. Ecology 85 (11), 2960–2970.

Humphries, S.E., Imberger, J., 1982. The influence of the internal structure and the dynamics of Burrinjuck reservoir on phytoplankton blooms. Environmental Dynamic Report ED 82-023. Centre for Water Research, University Western Australia, Perth, Australia.

Ibelings, B.W., Mur, L.R., Walsby, A.E., 1991. Diurnal changes in buoyancy and vertical distribution in populations of *Microcystis* in two shallow lakes. J. Plankton Res. 13 (2), 419–436.

Idso, S.B., 1973. On the concept of lake stability. Limnol. Oceanogr. 18 (4), 681–683.

Jöhnk, K.D., Huisman, J., Sharples, J., Sommeijer, B., Visser, P.M., Stroom, J.M., 2008. Summer heatwaves promote blooms of harmful cyanobacteria. Glob. Chang Biol. 14 (3), 495–512.

Kirillin, G., 2010. Modeling the impact of global warming on water temperature and seasonal mixing regimes in small temperate lakes. Boreal Environ. Res. 15, 279–293.

Li, M., Zhu, W., Guo, L., Hu, J., Chen, H., Xiao, M., 2016. To increase size or decrease density? Different *Microcystis* species has different choice to form blooms. Sci. Rep. 6, 37056.

Li, M., Xiao, M., Zhang, P., Hamilton, D.P., 2018. Morphospecies-dependent disaggregation of colonies of the cyanobacterium *Microcystis* under high turbulent mixing. Water Res. 141, 340–348.

Lin, L., Appiah-Sefah, G., Li, M., 2015. Using a laser particle analyzer to demonstrate relationships between wind strength and *Microcystis* colony size distribution in Lake Taihu, China. J. Freshw. Ecol. 30 (3), 425–433.

McVicar, T.R., Van Niel, T.G., Li, L.T., Roderick, M.L., Rayner, D.P., Ricciardulli, L., Donohue, R.J., 2008. Wind speed climatology and trends for Australia, 1975–2006: capturing the stilling phenomenon and comparison with near-surface reanalysis output. Geophys. Res. Lett. 35 (20).

Nakamura, T., Adachi, Y., Suzuki, M., 1993. Flotation and sedimentation of a single *Microcystis* floc collected from surface bloom. Water Res. 27 (6), 979–983.

O'Reilly, C.M., Alin, S.R., Plisnier, P.D., Cohen, A.S., McKee, B.A., 2003. Climate change decreases aquatic ecosystem productivity of Lake Tanganyika, Africa. Nature 424 (6950), 766–768.

O'Reilly, C.M., Sharma, S., Gray, D.K., Hampton, S.E., Read, J.S., Rowley, R.J., Schneider, P., Lenters, J.D., McIntyre, P.B., Kraemer, B.M., 2015. Rapid and highly variable warming of lake surface waters around the globe. Geophys. Res. Lett. 42 (24), 703–710, 10781.

O'Brien, K.R., Meyer, D.L., Waite, A.M., Ivey, G.N., Hamilton, D.P., 2004. Disaggregation of *Microcystis aeruginosa* colonies under turbulent mixing: laboratory experiments in a grid-stirred tank. Hydrobiologia 519 (1–3), 143–152.

Paerl, H.W., Huisman, J., 2008. Blooms like it hot. Science 320 (5872), 57–58.

Pinker, R., Laszlo, I., 1992. Global distribution of photosynthetically active radiation as observed from satellites. J. Clim. 5 (1), 56–65.

Qin, B., Yang, G., Ma, J., Wu, T., Li, W., Liu, L., Deng, J., Zhou, J., 2018. Spatiotemporal changes of cyanobacterial bloom in large shallow eutrophic Lake Taihu, China. Front. Microbiol. 9, 451.

Ranjbar, M.H., Hamilton, D.P., Etemad-Shahidi, A., Helfer, F., 2021. Individual-based modelling of cyanobacteria blooms: physical and physiological processes. Sci. Total Environ. 792, 148418.

Regel, R.H., Brookes, J.D., Ganf, G.G., Griffiths, R.W., 2004. The influence of experimentally generated turbulence on the Mash01 unicellular *Microcystis aeruginosa* strain. Hydrobiologia 517 (1), 107–120.

Reichwaldt, E.S., Ghadouani, A., 2012. Effects of rainfall patterns on toxic cyanobacterial blooms in a changing climate: between simplistic scenarios and complex dynamics. Water Res. 46 (5), 1372–1393.

Reynolds, C.S., Oliver, R.L., Walsby, A.E., 1987. Cyanobacterial dominance: the role of buoyancy regulation in dynamic lake environments. N. Z. J. Mar. Freshw. Res. 21 (3), 379–390.

Reynolds, C.S., 1989. Physical determinants of phytoplankton succession. In: Sommern, U (Ed.), Plankton Ecology. Springer, Berlin.

Reynolds, C.S., 1997. Vegetation Processes in the Pelagic: A model for Ecosystem Theory. Ecology Institute Oldendorf/Luhe, Germany.

Robarts, R., Zohary, T., 1984. *Microcystis aeruginosa* and underwater light attenuation in a hypertrophic lake (Hartbeespoort Dam, South Africa). J. Ecol. 1001–1017.

Robson, B.J., Hamilton, D.P., 2003. Summer flow event induces a cyanobacterial bloom in a seasonal Western Australian estuary. Mar. Freshw. Res. 54 (2), 139–151.

Rousso, B.Z., Bertone, E., Stewart, R.A., Hughes, S.P., Hobson, P., Hamilton, D.P., 2022. Cyanobacteria species dominance and diversity in three Australian drinking water reservoirs. Hydrobiologia 849 (6), 1453–1469.

Rowe, M.D., Anderson, E.J., Wynne, T.T., Stumpf, R.P., Fanslow, D.L., Kijanka, K., Vanderploeg, H.A., Strickler, J.R., Davis, T.W., 2016. Vertical distribution of buoyant *Microcystis* blooms in a Lagrangian particle tracking model for short-term forecasts in Lake Erie. J. Geophy. Res. Oceans 121 (7), 5296–5314.

Scheffer, M., Baveco, J., DeAngelis, D., Rose, K.A., van Nes, E., 1995. Super-individuals a simple solution for modelling large populations on an individual basis. Ecol. Model. 80 (2), 161–170. -3.

Sharma, S., Jackson, D.A., Minns, C.K., Shuter, B.J., 2007. Will northern fish populations be in hot water because of climate change? Glob. Chang Biol. 13 (10), 2052–2064.

Sokolova, E., Pettersson, T.J.R., Bergstedt, O., Hermansson, M., 2013. Hydrodynamic modelling of the microbial water quality in a drinking water source as input for risk reduction management. J. Hydrol. (Amst) 497, 15–23.

Syktus, J., Trancoso, R., Ahrens, D., Toombs, N., Wong, K., 2020. Terrest. Ecosyst. Res. Netw. (TERN)., and RCP4.5, Version 1.0.2..

Thomas, M.K., Litchman, E., 2016. Effects of temperature and nitrogen availability on the growth of invasive and native cyanobacteria. Hydrobiologia 763 (1), 357–369.

Vanderploeg, H.A., Liebig, J.R., Carmichael, W.W., Agy, M.A., Johengen, T.H., Fahnenstiel, G.L., Nalepa, T.F., 2001. Zebra mussel (*Dreissena polymorpha*) selective filtration promoted toxic *Microcystis* blooms in Saginaw Bay (Lake Huron) and Lake Erie. Canad. J. Fisher. Aquat. Sci. 58 (6), 1208–1221.

Visser, P.M., Ibelings, B.W., Bormans, M., Huisman, J., 2016. Artificial mixing to control cyanobacterial blooms: a review. Aquat. Ecol. 50 (3), 423–441.

Wallace, B.B., Bailey, M.C., Hamilton, D.P., 2000. Simulation of vertical position of buoyancy regulating *Microcystis aeruginosa* in a shallow eutrophic lake. Aquat. Sci. 62 (4), 320–333.

Wang, C., Feng, T., Wang, P., Hou, J., Qian, J., 2017. Understanding the transport feature of bloom-forming *Microcystis* in a large shallow lake: a new combined hydrodynamic and spatially explicit agent-based modelling approach. Ecol. Model. 343, 25–38.

Williamson, C.E., Salm, C., Cooke, S.L., Saros, J.E., 2010. How do UV radiation, temperature, and zooplankton influence the dynamics of alpine phytoplankton communities? Hydrobiologia 648 (1), 73–81.

Winslow, L., Read, J., Woolway, R., Brentrup, J., Leach, T., Zwart, J., Albers, S., Collinge, D., 2019. Package 'rLakeAnalyzer'. The Comprehensive R Archive Network.

Wood, J.E., Silverman, J., Galanti, B., Biton, E., 2020. Modelling the distributions of desalination brines from multiple sources along the Mediterranean coast of Israel. Water Res. 173, 115555.

Wood, S.A., Puddick, J., Borges, H., Dietrich, D.R., Hamilton, D.P., 2015. Potential effects of climate change on cyanobacterial toxin production. In: Botana, LM, Louzao, C, Vilarino, N (Eds.), Climate Change and Marine and Freshwater Toxins. Walter de Gruyter Publishers, Berlin.

Woolway, R.I., Meinson, P., Nõges, P., Jones, I.D., Laas, A., 2017. Atmospheric stilling leads to prolonged thermal stratification in a large shallow polymictic lake. Climat. Change 141 (4), 759–773.

Woolway, R.I., Merchant, C.J., 2019. Worldwide alteration of lake mixing regimes in response to climate change. Nat. Geosci. 12 (4), 271–276.

Wu, X., Kong, F., 2009. Effects of light and wind speed on the vertical distribution of *Microcystis aeruginosa* colonies of different sizes during a summer bloom. Int. Rev. Hydrobiol. 94 (3), 258–266.

Wu, X., Yang, T., Feng, S., Li, L., Xiao, B., Song, L., Sukenik, A., Ostrovsky, I., 2020. Recovery of *Microcystis* surface scum following a mixing event: insights from a tank experiment. Sci. Total Environ. 728, 138727.

Wynne, T.T., Stumpf, R.P., Tomlinson, M.C., Fahnenstiel, G.L., Dyble, J., Schwab, D.J., Joshi, S.J., 2013. Evolution of a cyanobacterial bloom forecast system in western Lake Erie: development and initial evaluation. J. Great Lakes Res. 39, 90–99.

Xiao, M., Willis, A., Burford, M.A., Li, M., 2017. Review: a meta-analysis comparing cell-division and cell-adhesion in *Microcystis* colony formation. Harmful Algae 67, 85–91.

Xiao, M., Li, M., Reynolds, C.S., 2018. Colony formation in the cyanobacterium *Microcystis*. Biolog. Rev. 93 (3), 1399–1420.

Xiao, M., Li, M., Duan, P., Qu, Z., Wu, H., 2019. Insights into the relationship between colony formation and extracellular polymeric substances (EPS) composition of the cyanobacterium *Microcystis* spp. Harmful Algae 83, 34–41.

Xiao, M., Hamilton, D.P., O'Brien, K.R., Adams, M.P., Willis, A., Burford, M.A., 2020. Are laboratory growth rate experiments relevant to explaining bloom-forming cyanobacteria distributions at global scale? Harmful Algae 92, 101732.

Yang, Z., Kong, F., Shi, X., Zhang, M., Xing, P., Cao, H., 2008. Changes in the morphology and polysaccharide content of *Microcystis aeruginosa* (cyanobacteria) during flagellate grazing. J. Phycol. 44 (3), 716–720.

Yao, B., Liu, Q., Gao, Y., Cao, Z., 2017. Characterizing vertical migration of *Microcystis aeruginosa* and conditions for algal bloom development based on a light-driven migration model. Ecol. Res. 32 (6), 961–969.

Zhang, F., Zhang, H., Bertone, E., Stewart, R., Lemckert, C., Cinque, K., 2020. Numerical study of the thermal structure of a stratified temperate monomictic drinking water reservoir. J. Hydrol. 30, 100699.